Available online at www.sciencedirect.com
ScienceDirect
Physica B 394 (2007) 221–228
PHYSICA B
www.elsevier.com/locate/physb

Manipulating light with photonic crystals

Shanhui Fan

Department of Electrical Engineering and Ginzton Laboratory, Stanford University, Stanford, CA 94305, USA

Abstract

We review some of the recent advances in the theory of photonic crystals, drawing examples from our own work in magneto-optical and dynamic photonic crystals. The combination of theory and simulations shows that these crystal structures exhibit rich optical physics effects, and can provide new ways to accomplish sophisticated optical information processing tasks.
© 2007 Published by Elsevier B.V.

PACS: 42.70.Qs

Keywords: Photonic crystals; Magneto-optical crystals; Dynamic crystals; Computational techniques; Band diagrams; Analytical models

1. Introduction

There has been great interest in designing wavelength-scale or even deep sub-wavelength scale structures in order to enable new functionalities for optical information processing [1,2]. In this paper, we review some of our own recent works along this direction. Examples given here include analysis of magneto-optical [3–5] as well as dynamic photonic crystals [6–11]. These structures are designed towards accomplishing tasks such as signal isolation and buffering, which are critically important for creating large-scale on-chip optical circuits.

2. Magneto-optical photonic crystals

One of the most fundamental challenges to the creation of on-chip, large-scale integrated optics has been to provide signal isolation and to suppress parasitic reflections between devices. In this context, there is a very strong interest in the miniaturization of nonreciprocal optical devices and their on-chip integration [12–14]. Due to the weakness of magneto-optical effects, conventional devices require a long propagation distance and occupy a large footprint. Thus, it should be very fruitful to explore the enhancement of magneto-optical effects in photonic crystals [15,16], for the purpose of creating ultra-compact devices with enhanced functionalities.

We start by considering the modal properties of micro-cavities incorporating magneto-optical materials. At optical wavelengths, the property of a magneto-optical material is typically characterized by a gyrotropic dielectric tensor $\overleftrightarrow{\varepsilon}$ [17]:

$$D = \overleftrightarrow{\varepsilon}\, E = \varepsilon_0 E + j\varepsilon_a \hat{M} \times E \equiv (\varepsilon_0 + \overleftrightarrow{\varepsilon'})E, \tag{1}$$

where ε_0 is the dielectric constant in the absence of magnetization, ε_a measures the strength of the magneto-optical effects, and $\hat{M}$ is the unit vector indicating the direction of magnetization. (Below, for concreteness, we assume a magnetization along the z direction.) The strength of magneto-optical effects is measured by the Voigt parameter $Q_M = \varepsilon_a/\varepsilon_0$. For most transparent materials, the Voigt parameter is typically less than 10^{-3} [17].

To theoretically describe modes in a magneto-optical photonic crystal system, we expand to first order in ε_a the master equations for photonic crystals [18] that describes the magnetic field H in the steady state at an angular frequency ω, to obtain

$$\Theta|H\rangle = \nabla \times \frac{1}{\varepsilon_0}\nabla \times |H\rangle - \nabla \times \frac{\overleftrightarrow{\varepsilon'}}{\varepsilon_0^2}\nabla \times |H\rangle = \left(\frac{\omega}{c}\right)^2 |H\rangle. \tag{2}$$

E-mail address: shanhui@stanford.edu.

0921-4526/$ - see front matter © 2007 Published by Elsevier B.V.
doi:10.1016/j.physb.2006.12.078

In Eq. (2), $\Theta_0 \equiv \nabla \times (1/\varepsilon_0)\nabla\times$ describes a photonic crystal in the absence of magneto-optical effects. The effects of magneto-optics can now be treated in terms of the coupling of eigen-modes of Θ_0 as induced by the perturbation $V \equiv -\nabla \times (\overleftrightarrow{\varepsilon}'/\varepsilon_0^2)\nabla\times$. For two normalized eigen-modes $|H_{1,2}\rangle$ for Θ_0 at eigen-frequencies $\omega_{1,2}$, the coupling constant between them as induced by V can be calculated as

$$V_{12} \equiv \langle H_1|V|H_2\rangle = -\int H_1^* \cdot \nabla \times \frac{\overleftrightarrow{\varepsilon}'}{\varepsilon_0^2}\nabla \times H_2 = \omega_1\omega_2 \int j\varepsilon_a \hat{M} \cdot (E_1^* \times E_2). \quad (3)$$

As a concrete example, we consider a two-dimensional crystal shown in Fig. 1 [3]. The structure consists of a triangular lattice of air holes in bismuth iron garnet. The air holes have a radius of $0.35a$, where a is the lattice constant. The corresponding nonmagnetic photonic crystal exhibits a large band gap for TE modes that have electric field polarized in the plane. Filling one of the air holes creates a pair of degenerate dipole modes in the photonic band gap. These two modes can be categorized as an even mode $|e\rangle$ (Fig. 1(a)) and an odd mode $|o\rangle$ (Fig. 1(b)) with respect to a mirror plane of the crystal.

In the presence of magneto-optical materials, the two modes $|e\rangle$ and $|o\rangle$ couple with each other. The system is now described by a 2×2 matrix

$$\Theta = \begin{pmatrix} \omega_e^2 & V_{eo} \\ -V_{eo} & \omega_o^2 \end{pmatrix}. \quad (4)$$

Since the two modes are standing waves that possess real-valued electric fields, the coupling constant V_{eo} as described by Eq. (3) is purely imaginary. For this system, which has C_{6v} symmetry, $\omega_e = \omega_o \equiv \omega_0$. With the presence of magneto-optical materials in the cavity, the eigen-modes of the systems, denoted as $|+\rangle$ and $|-\rangle$, now take the form of a rotating wave:

$$|\pm\rangle = |e\rangle \pm i|o\rangle, \quad (5)$$

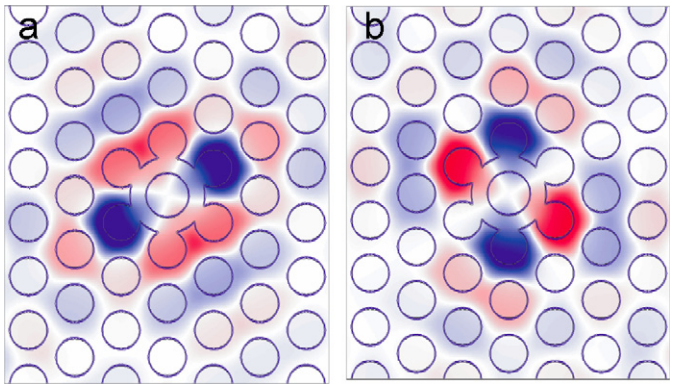

Fig. 1. (a) and (b): A pair of doubly degenerate defect states in a two-dimensional photonic crystal. The crystal consists of an array of air holes introduced into a high dielectric material. Red and blue represent large positive or negative magnetic fields.

with the frequencies located at

$$\omega_\pm = \omega_0 \pm \frac{|V_{eo}|}{2\omega_0}. \quad (6)$$

The above modal analysis reveals some of the most interesting properties about magneto-optical photonic crystals in general:

(1) Time-reversal symmetry breaking. Since the two counter-rotating modes $|\pm\rangle$ are related by a time-reversal operation, the frequency splitting between them clearly indicates the breaking of time-reversal symmetry and reciprocity.
(2) Fundamental suppression of the effects of disorder by time-reversal symmetry breaking. Even in the case where ω_e deviates from ω_o, for example, due to fabrication-related disorder that breaks the three-fold rotational symmetry, as long as the magneto-optical coupling is sufficiently strong, i.e. $|V_{eo}| \gg |\omega_e - \omega_o|\omega_e$, $|e\rangle \pm i|o\rangle$ remain the eigen-states of the system. Thus, in the limit of strong magneto-optical coupling, the rotating waveform of the eigen-modes is independent of the slight structural disorders that would almost always occur in practical devices.

Exploiting the unique modal properties of rotating states inside a magneto-optical photonic crystal cavity, we design a four-port circulator as shown in Fig. 2. The system consists of a bus and a drop waveguide, both evanescently coupled to the resonator. Magneto-optical materials are introduced to create circularly rotating modes in opposite directions at different frequencies in the cavity. When the magneto-optically induced frequency splitting between the two rotating modes exceeds the cavity linewidth that results from the cavity-waveguide coupling, the device functions as an optical circulator that provides optical signal isolation. Light incident from the waveguide in the lower half of the structure, with a frequency coincide with the counter-clockwise resonance in the cavity, is completely transferred to other waveguide (Fig. 2(a)). In the time-reversed scenario, the incident light through the upper waveguide remains un-transferred since the clockwise rotating resonance in the cavity has a different frequency (Fig. 2(b)). The device footprint is on the single-micron scale and the device is readily integrated with other planar components.

The nonreciprocal transport property is fundamentally protected against the effects of disorders. To highlight this, we have designed the circulator structure, such that the device functions as an ideal add-drop filter, when the off-diagonal part of the matrix elements in the dielectric tensor is set to zero. In such a reciprocal add/drop filter, the ideal 100% transfer efficiency relies upon creating rotating states from a linear superposition of two degenerate standing wave modes having the same frequency and linewidth [19]. Preserving the degeneracy condition of the standing wave modes translates to stringent tolerance requirements. This

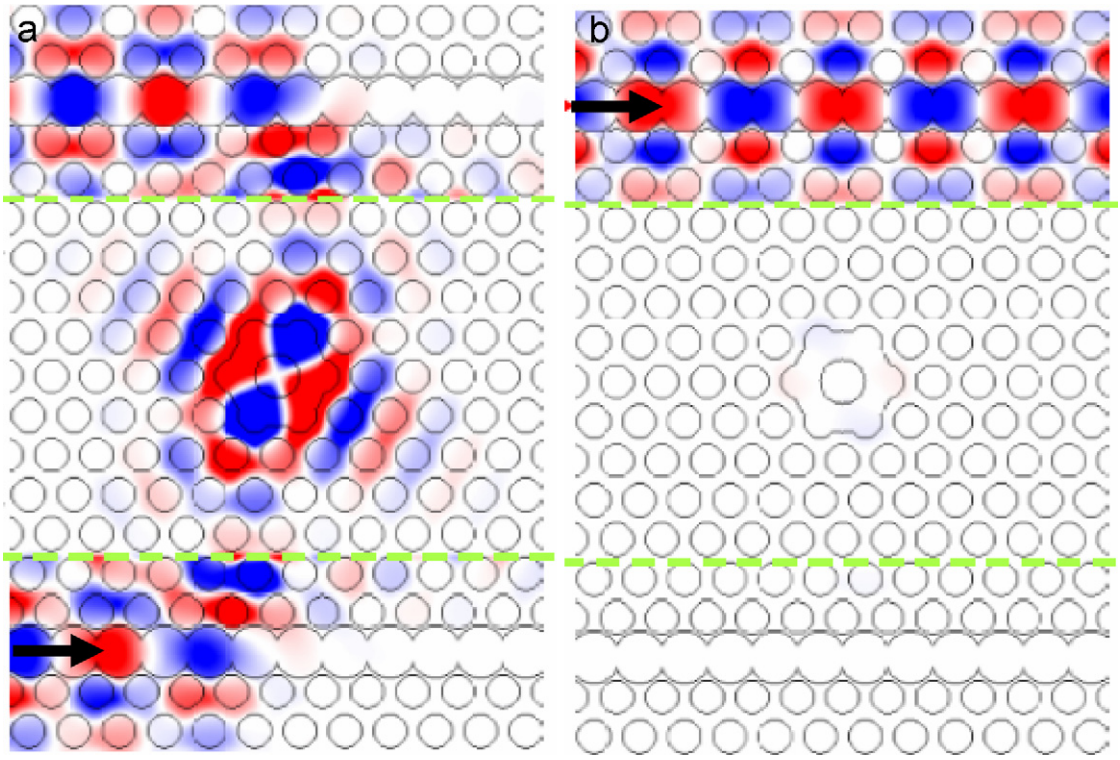

Fig. 2. Operation of a photonic crystal circulator, constructed by coupling the magneto-optical cavity as shown in Fig. 1 to two waveguides. Shown here are steady state field distributions when the incident light is in resonance with the counter-clockwise rotating state. Red and blue represent large positive or negative fields. The arrows indicate the direction of the incident light. The field between two dashed lines is plotted with a different saturation such that fields in both waveguides and cavities can be seen.

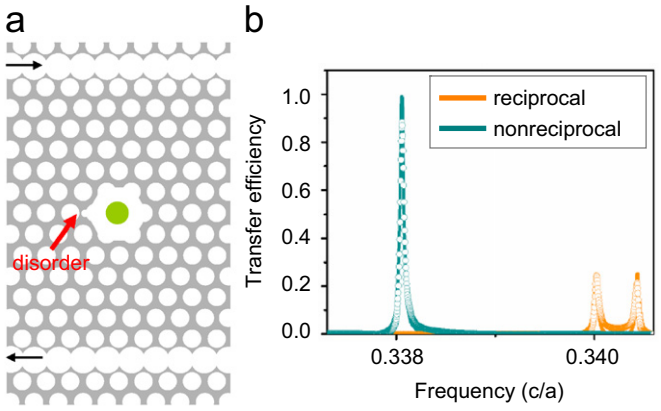

Fig. 3. (a) A photonic crystal circulator structure with two waveguides side coupled to a cavity at the center. The green region at the center of the cavity consists of magneto-optical material. In the absence of the disorder, in the form of a small bump at the side the cavity, both the circulator structure, and its fictitious reciprocal counter part, created by removing the off-diagonal part of the dielectric tensor, give ideal transfer efficiency between the waveguides at resonance. The black arrows represent the direction of transfer. (b) Comparison of the transfer property of the circulator and its reciprocal counter part, in the presence of the disorder.

is demonstrated in Fig. 3, where as an example of disorder we introduce small bump on the side of the cavity. For the reciprocal structure, such a disorder reduces the transfer efficiency between the waveguides from 100% to 25%, and causes strong reflection in the incoming waveguide. In the nonreciprocal structure, on the other hand, the peak transmission efficiency remains very close to 100% in spite of the disorder [5]. We believe that exploring the interplay between time-reversal symmetry breaking and disorder to be a particularly exciting area, which can potentially lead to regimes of photon propagation that are completely absent in reciprocal structures.

3. Dynamic photonic crystals and stopping light

The idea of dynamic photonic crystal is to modulate the property of a crystal while a photon pulse is inside the crystal. In doing so, the spectrum of the pulse can be molded almost arbitrarily [6,20], leading to highly non-trivial information processing capabilities on chip.

3.1. Control the spectrum of light with dynamics

As a simple example illustrating the general aspects of dynamics, consider a linearly polarized electromagnetic wave in one dimension, the wave equation for the electric field is

$$\frac{\partial^2 E}{\partial x^2} - (\varepsilon_0 + \varepsilon(t))\mu_0 \frac{\partial^2 E}{\partial t^2} = 0. \quad (7)$$

Here, $\varepsilon(t)$ represents the modulation and ε_0 is the background dielectric constant. We assume that both ε_0 and $\varepsilon(t)$

are independent of position. Hence different wavevector components do not mix in the modulation process. Consider a specific wavevector component at k_0, with electric field described by $E(t) = f(t)e^{i(\omega_0 t - k_0 x)}$, where $\omega_0 = \left(k_0/(\sqrt{\mu_0 \varepsilon_0})\right)$. By using a slowly varying envelope approximation, and by further assuming that the index modulations are weak, i.e. $\varepsilon(t) = \varepsilon_0$, Eq. (7) can be simplified as

$$i\frac{\partial f}{\partial t} = \frac{\varepsilon(t)\omega_0}{2[\varepsilon(t)+\varepsilon_0]} f \approx \frac{\varepsilon(t)\omega_0}{2\varepsilon_0} f, \tag{8}$$

which has an exact analytical solution

$$f(t) = f(t_0)\exp\left[-i\omega_0 \int_{t_0}^{t} \frac{\varepsilon(t')}{2\varepsilon_0}\, dt'\right], \tag{9}$$

where t_0 is the starting time of the modulation. Thus the "instantaneous frequency" of the electric field for this wavevector component is

$$\omega(t) = \omega_0\left(1 - \frac{\varepsilon(t)}{2\varepsilon_0}\right). \tag{10}$$

We note that frequency change is proportional to the magnitude of the refractive index shift alone. Thus, the process defined here differs in a fundamental way from traditional nonlinear optical processes, in that, regardless of how slow the modulation is, as long as light is in the system, the frequency shift can always be accomplished.

3.2. Stopping light

Here we will demonstrate important consequence of the dynamic process discussed in the previous section, in its application for stopping a light pulse. By stopping light, we aim to reduce the group velocity of a light pulse to zero, while completely preserving all the coherent information encoded in the pulse. Such ability holds the key to the ultimate control of light, and has profound implications for optical communications and quantum information processing [21,22].

There has been extensive work attempting to control the speed of light using optical resonances in static photonic crystal structures [23–27]. Nevertheless, such structures are fundamentally limited by the delay-bandwidth product constraint—the group delay from an optical resonance is inversely proportional to the bandwidth within which the delay occurs [28,29]. Therefore, for a given optical pulse with a certain temporal duration and corresponding frequency bandwidth, the minimum group velocity achievable is limited.

To stop light, it is necessary to use a dynamic system. The general condition for stopping light [6] is illustrated in Fig. 4. Imagine a dynamic photonic crystal system, with an initial bandstructure possessing a sufficiently wide bandwidth. Such a state is used to accommodate an incident pulse, for which each frequency component occupies a unique wavevector component. After the pulse has entered the system, one can then stop the pulse by flattening the dispersion relation of the crystal adiabatically, while preserving the translational invariance. In doing so, the spectrum of the pulse is compressed, and its group velocity is reduced. In the meantime, since the translational symmetry is still preserved, the wavevector components of the pulse remain unchanged, and thus one actually preserves the dimensionality of the phase space. This is crucial in preserving all the coherent information encoded in the original pulse during the dynamic process.

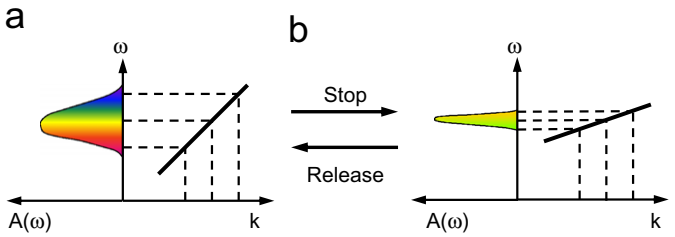

Fig. 4. The general conditions for stopping a light pulse. (a) The large-bandwidth state that is used to accommodate an incident light pulse. (b) The narrow-bandwidth state that is used to hold the light pulse. An adiabatic transition between these two states stops a light pulse inside the system.

To create a dynamic photonic crystal, one needs to adjust its properties as a function of time. However, the amount of refractive index tuning that can be accomplished with standard optoelectronics technology is generally quite small, with a fractional change typically on the order of $((\delta n)/n) \sim 10^{-4}$. Therefore, we employ Fano interference schemes in which a small refractive index modulation leads to a very large change of the bandwidth of the system. The essence of Fano interference scheme is the presence of multi-path interference, where at least one of the paths includes a resonant tunneling process [30]. Such interference can be used to greatly enhance the sensitivity of resonant devices to small refractive index modulation [31,32].

Here we consider a waveguide side coupled to two cavities [33]. The cavities have resonant frequencies $\omega_{A,B} \equiv \omega_0 \pm (\delta\omega/2)$. (This system represents an all-optical analogue of atomic systems exhibiting electromagnetically induced transparency (EIT) [34,35].) For simplicity, we assume that the cavities couple to the waveguide with equal rate of γ. The transmission and reflection coefficients ($t_{A,B}$ and $r_{A,B}$, respectively) in the waveguide with a single-side cavity can be derived [36] as

$$t_{A,B} = \frac{j(\omega - \omega_{A,B})}{j(\omega - \omega_{A,B}) + \gamma}, \tag{11}$$

$$r_{A,B} = \frac{\gamma}{j(\omega - \omega_{A,B}) + \gamma}. \tag{12}$$

When two cavities are cascaded together, the transmission spectrum becomes [37]

$$T = \left(\frac{|t_A t_B|}{1-|r_A r_B|}\right)^2 \frac{1}{1+4\left(\left(\sqrt{|r_A r_B|}\right)/(1-|r_A r_B|)\right)^2 \sin^2\theta}. \quad (13)$$

Here, θ is one-half the round trip phase accumulated in the waveguides: $\theta = \frac{1}{2}\mathrm{Arg}(r_A r_B e^{-2j\beta(\omega)L_1})$, where $\beta(\omega)$ is the waveguide dispersion relationship and L_1 is the spacing between the cavities.

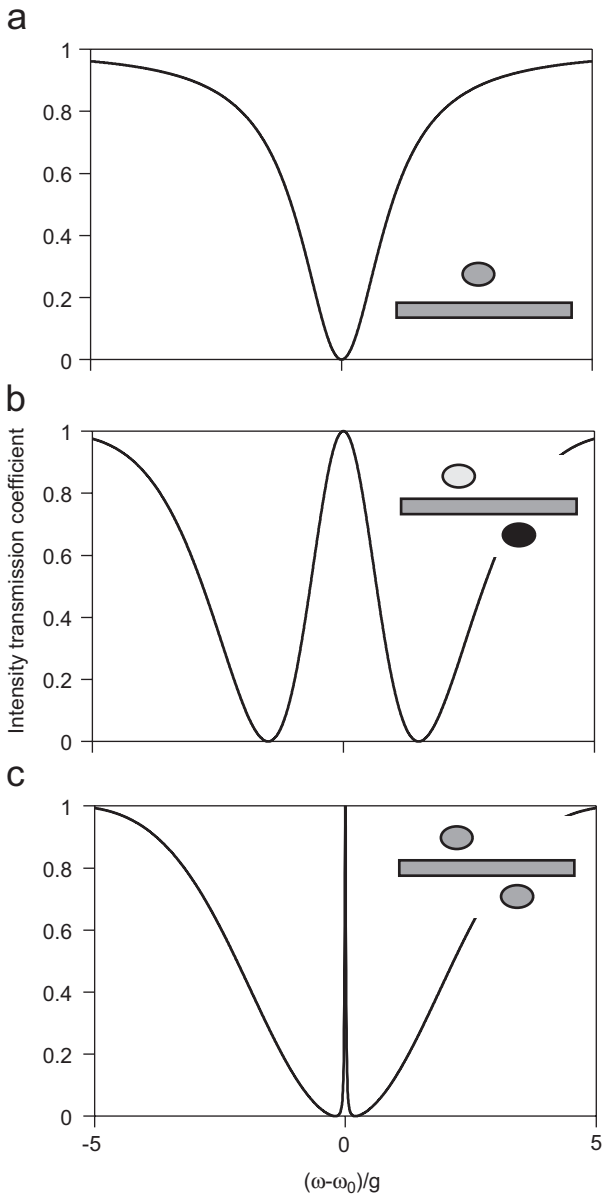

Fig. 5. (a) Transmissions spectrum through a waveguide side coupled to a single-mode cavity. (b) and (c) Transmission spectra through a waveguide side coupled to two cavities. The spectra are calculated using Eqs. (11)–(13). The parameters for the cavities are: $\omega_0 = (2\pi c)/L_1$ and $\gamma = 0.05\omega_0$. The waveguide satisfies a dispersion relation $\beta(\omega) = \omega/c$, where c is the speed of light in the waveguide, and L_1 is the distance between the cavities. In (b), $\omega_{a,b} = \omega_0 \pm 1.5\gamma$. In (c), $\omega_{a,b} = \omega_0 \pm 0.2\gamma$.

The transmission spectra of one- and two-cavity structures, calculated using Eqs. (11)–(13), are plotted in Fig. 5. In the case of one-cavity structure, the transmission features a dip in the vicinity of the resonant frequency, with the width of the dip controlled by the strength of waveguide-cavity coupling (Fig. 5(a)). With two cavities, when the condition

$$2\beta(\omega_0)L = 2n\pi \quad (14)$$

is satisfied, the transmission spectrum features a peak centered at ω_0. The width of the peak is highly sensitive to the frequency spacing between the resonances $\delta\omega$. When the cavities are lossless, the center peak can be tuned from a wide peak when $\delta\omega$ is large (Fig. 5(b)), to a peak that is arbitrarily narrow with $\delta\omega \to 0$ (Fig. 5(c)). The two-cavity structure, appropriately designed, therefore behaves as a tunable bandwidth filter, as well as a tunable delay element, in which the bandwidth can be in principle adjusted by any order of magnitude with very small refractive index modulation.

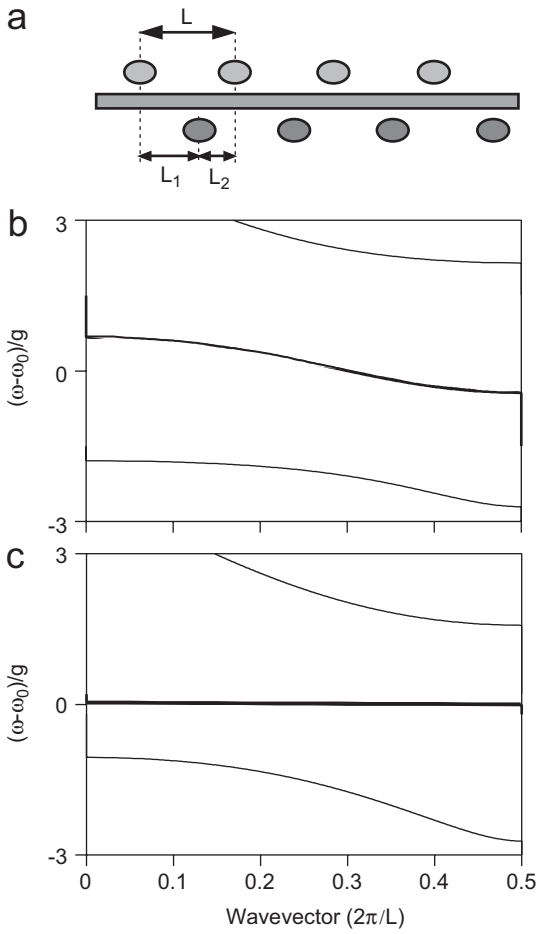

Fig. 6. (a) Schematic of a coupled-cavity structure used to stop light, (b) and (c), band structures for the system shown in (a), as the frequency separation between the cavities are varied, using the same waveguide and cavity parameters as in Figs. 5(b) and (c), with the additional parameter $L_2 = 0.7L_1$. The thicker lines highlight the middle band that will be used to stop a light pulse.

By cascading the tunable bandwidth filter structure as described above, one can construct a structure that is capable of stopping light (Fig. 6(a)). In such a light-stopping structure, the photonic band diagram becomes highly sensitive to small refractive index modulation.

The photonic bands for the structure in Fig. 6(a) can be calculated using a transmission matrix method. The transmission matrix for a waveguide side coupled to a single resonator with resonance frequency ω_i can be calculated as [36]:

$$T_{c_i} = \begin{pmatrix} 1 + j\gamma/(\omega - \omega_i) & j\gamma/(\omega - \omega_i) \\ -j\gamma/(\omega - \omega_i) & 1 - j\gamma/(\omega - \omega_i) \end{pmatrix}. \quad (15)$$

The transmission matrix through an entire unit cell in Fig. 6 can then be determined as

$$T = T_{c_1} T_{l_1} T_{c_2} T_{l_2}, \quad (16)$$

where

$$T_{l_i} = \begin{pmatrix} e^{-j\beta L_i} & 0 \\ 0 & e^{j\beta L_i} \end{pmatrix}$$

is the transmission matrix for a waveguide section of length L_i. Here, β is the wavevector of the waveguide at a given frequency ω. From this, we obtain the band diagram of the system as [8]

$$\frac{1}{2}\mathrm{Tr}(T) = \cos(kL) = f(\omega) \equiv \cos(\beta L) + \frac{C_+}{(\omega - \omega_A)} + \frac{C_-}{(\omega - \omega_B)}, \quad (17)$$

where

$$C_\pm = \gamma \sin(\beta L) \pm \gamma^2 \frac{2\sin(\beta L_1)\sin(\beta L_2)}{(\omega_A - \omega_B)}.$$

The band diagrams thus calculated are shown in Fig. 6, in which the waveguide and cavity parameters are the same as those used to generate the transmission spectrum in Fig. 5. In the vicinity of the resonances, the system supports three photonic bands, with two gaps occurring around ω_A and ω_B. The width of the middle band depends strongly on the resonant frequencies ω_A and ω_B. By modulating the frequency spacing between the cavities, one goes from a system with a large bandwidth (Fig. 6(b)), to a system with a very narrow bandwidth (Fig. 6(c)). In fact, it can be analytically proved that the system can support a band that is completely flat in the entire first Brillouin zone [8], allowing a light pulse to be frozen inside the structure with the group velocity reduced to zero.

The system presented above can be implemented in a photonic crystal of a square lattice of dielectric rods ($n = 3.5$) with a radius of $0.2a$, (a is the lattice constant) embedded in air ($n = 1$) [8] (Fig. 7). The photonic crystal possesses a band gap for TM modes with electric field parallel to the rod axis. Removing one row of rods along the pulse propagation direction generates a single-mode waveguide. Decreasing the radius of a rod to $0.1a$ and the

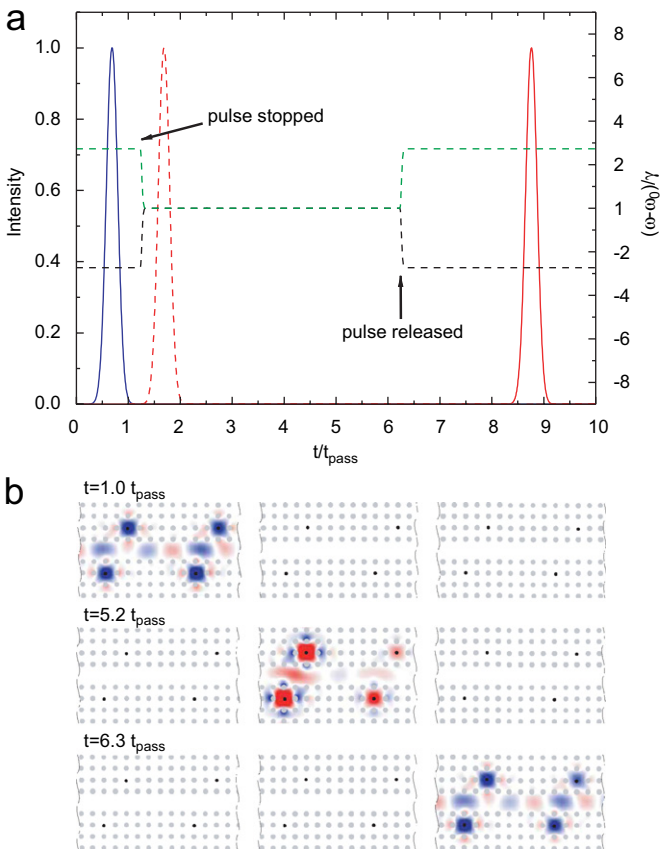

Fig. 7. Light-stopping process in a photonic crystal simulated using finite-difference time-domain methods. The crystal consists of a waveguide side coupled to 100 cavity pairs. Fragments of the photonic crystal are shown in part (b). The three fragments correspond to unit cells 12–13, 55–56, 97–98. The dots indicate the positions of the dielectric rods. The black dots represent the cavities. (a) The dashed green and black lines represent the variation of ω_A and ω_B as a function of time, respectively. The blue solid line is the intensity of the incident pulse as recorded at the beginning of the waveguide. The red dashed and solid lines represent the intensity at the end of the waveguide, in the absence and the presence of modulation, respectively. t_{pass} is the passage time of the pulse in the absence of modulation. (b) Snapshots of the electric field distributions in the photonic crystal at the indicated times. Red and blue represent large positive and negative electric fields, respectively. The same color scale is used for all the panels.

dielectric constant to $n = 2.24$ provides a single-mode cavity. The nearest-neighbor cavities are separated by a distance of $l_1 = 2a$ along the propagation direction, and the unit cell periodicity is $l = 8a$. The waveguide-cavity coupling occurs through barrier of one rod. The resonant frequencies of the cavities are tuned by refractive index modulation of the cavity rods.

We simulate the entire process of stopping light for $N = 100$ pairs of cavities with finite-difference-time-domain (FDTD) method, which solves Maxwell's equations without approximation. The dynamic process for stopping light is shown in Fig. 7. We generate a Gaussian pulse in the waveguide (the process is independent of the pulse shape). The excitation reaches its peak at $t = 0.8t_{pass}$, where t_{pass} is the traversal time of the pulse through the

static structure. During the pulse generation, the cavities have a large frequency separation. The field is concentrated in both the waveguide and the cavities (Fig. 7(b), $t = 1.0t_{pass}$), and the pulse propagates at a relatively high speed of $v_g = 0.082c$. After the pulse is generated, we gradually reduce the frequency separation Δ to zero. During this process, the speed of light is drastically reduced to zero. As the bandwidth of the pulse is reduced, the field concentrates in the cavities (Fig. 7(b), $t = 5.2t_{pass}$). When zero group velocity is reached, the photon pulse can be kept in the system as a stationary waveform for any time duration. In this simulation, we store the pulse for a time delay of $5.0t_{pass}$, and then release the pulse by repeating the same index modulation in reverse (Fig. 7(b), $t = 6.3t_{pass}$). The pulse intensity as a function of time at the right end of the waveguide is plotted in Fig. 7(a), and shows the same temporal shape as both the pulse that propagates through the un-modulated system, and the initial pulse recorded at the left end of the waveguide. Thus, the pulse is perfectly recovered without distortion after the intended delay.

In the all-optical light-stopping scheme presented above, for a small refractive index shift of $\delta n/n = 10^{-4}$ achievable in practical optoelectronic devices, and assuming a carrier frequency of approximately 200 THz, as used in optical communications, the achievable bandwidths are on the order of 20 GHz, which is comparable to the bandwidth of a single-wavelength channel in high-speed optical systems. The storage times are limited only by the cavity lifetimes, which may eventually approach millisecond time scales as limited by residual loss in transparent materials. With such performance, the capabilities for on-chip stopping light should have important implications for optical communication systems. As an important step towards its eventual experimental demonstration, the required EIT-like two-cavity interference effects have recently been observed in a micro-ring cavity system on a silicon chip [37]. The general concept of introducing dynamics into photonic crystal systems could also be very promising for creating new optical signal processing functionalities far beyond the capabilities of static systems.

4. Concluding remarks

In this paper we review some of the recent developments in the theory of photonic crystals, drawing examples from our own recent work on magneto-optical as well as dynamic crystal structures. These developments highlight two general trends in the theoretical work in this field. On one hand, using computational electromagnetics techniques such as the FDTD methods [38] in combination with modern large-scale computing architectures, almost any complex optical processes in photonic crystal can now be simulated through exact numerical solutions of Maxwell's equations. On the other hand, with the band structures and modal properties of passive dielectric photonic structures largely mapped out, one can now create analytical models with only a few dynamic variables based upon these modal properties, in order to describe the essential physics of optical processes in photonic crystals. These developments in both theory and simulations, in the context of very rapid progress in experimental fabrications of photonic crystals, are leading to ways of controlling light that are truly unprecedented.

Acknowledgments

The work is supported in part by NSF and DARPA. The author acknowledges the important contributions of members of Fan's group at Stanford, especially M.F. Yanik, Z. Wang, M.L. Povinelli, and S. Sandhu, to the works presented here.

References

[1] E. Yablonovitch, Phys. Rev. Lett. 58 (1987) 2059.
[2] S. John, Phys. Rev. Lett. 58 (1987) 2486.
[3] Z. Wang, S. Fan, Appl. Phys. B 81 (2005) 369.
[4] Z. Wang, S. Fan, Opt. Lett. 30 (2005) 1989.
[5] Z. Wang, S. Fan, Photon. Nanostruct. Fundam. Appl. 4 (2006) 132.
[6] M.F. Yanik, S. Fan, Phys. Rev. Lett. 92 (2004) (Art. No. 083901).
[7] M.F. Yanik, S. Fan, Phys. Rev. Lett. 93 (2004) (Art. No. 173903).
[8] M.F. Yanik, W. Suh, Z. Wang, S. Fan, Phys. Rev. Lett. 93 (2004) (Art. No. 233903).
[9] M.F. Yanik, S. Fan, Phys. Rev. A 71 (2005) (Art. No. 013803).
[10] M.F. Yanik, S. Fan, Studies Appl. Math. 115 (2005) 233.
[11] S. Sandhu, M.L. Povinelli, M.F. Yanik, S. Fan, Opt. Lett. 31 (2006) 1985.
[12] M. Levy, IEEE J. Sel. Top. Quantum Electron. 8 (2002) 1300.
[13] R.L. Espinola, T. Izuhara, M. Tsai, R.M. Osgood, H. Dotsch, Opt. Lett. 29 (2004) 941.
[14] H. Yokoi, Y. Shoji, E. Shin, T. Mizumoto, Appl. Opt. 43 (2004) 4745.
[15] M. Inoue, K. Arai, T. Fujii, M. Abe, J. Appl. Phys. 85 (1999) 5768.
[16] M.J. Steel, M. Levy, R.M. Osgood, IEEE Photon. Technol. Lett. 12 (2000) 1171.
[17] A.K. Zvezdin, V.A. Kotov, Modern Magnetooptics and Magnetooptical Materials, Institute of Physics Publishers, Bristol, 1997.
[18] J.D. Joannopoulos, R.D. Meade, J.N. Winn, Photonic Crystals: Molding the Flow of Light, Princeton University Press, Princeton, NJ, 1995.
[19] S. Fan, P.R. Villeneuve, J.D. Joannopoulos, H.A. Haus, Phys. Rev. Lett. 80 (1998) 960.
[20] E.J. Reed, M. Soljacic, J.D. Joannopoulos, Phys. Rev. Lett. 91 (2003) (Art. No.133901).
[21] C. Liu, Z. Dutton, C.H. Behroozi, L.V. Hau, Nature 409 (2001) 490.
[22] D.F. Phillips, A. Fleischhauer, A. Mair, R.L. Walsworth, M.D. Lukin, Phys. Rev. Lett. 86 (2001) 783.
[23] M. Notomi, K. Yamada, A. Shinya, J. Takahashi, C. Takahashi, I. Yokoyama, Phys. Rev. Lett. 87 (2001) (Art. No. 253902).
[24] N. Stefanou, A. Modinos, Phys. Rev. B 57 (1998) 12127.
[25] A. Yariv, Y. Xu, R.K. Lee, A. Scherer, Opt. Lett. 24 (1999) 711.
[26] M. Bayindir, B. Temelkuran, E. Ozbay, Phys. Rev. Lett. 84 (2000) 2140.
[27] Y.A. Vlasov, M. O'Boyle, H.F. Harmann, S.J. McNab, Nature 438 (2005) 65.
[28] G. Lenz, B.J. Eggleton, C.K. Madsen, R.E. Slusher, IEEE J. Quantum Electron. 37 (2001) 525.
[29] Z. Wang, S. Fan, Phys. Rev. E 68 (2003) (Art. No. 066616).
[30] U. Fano, Phys. Rev. 124 (1961) 1866.
[31] S. Fan, Appl. Phys. Lett. 80 (2002) 910.
[32] S. Fan, W. Suh, J.D. Joannopoulos, J. Opt. Soc. Am. A 20 (2003) 569.
[33] W. Suh, Z. Wang, S. Fan, IEEE J. Quantum Electron. 40 (2004) 1511.

[34] S.E. Harris, Phys. Today 50 (1997) 36.
[35] L. Maleki, A.B. Matsko, A.A. Savchenkov, V.S. Ilchenko, Opt. Lett. 29 (2004) 626.
[36] S. Fan, P.R. Villeneuve, J.D. Joannopoulos, C. Manalatou, M.J. Khan, H.A. Haus, Phys. Rev. B 59 (1999) 15882.
[37] Q. Xu, S. Sandhu, M.L. Povinelli, J. Shakya, S. Fan, M. Lipson, Phys. Rev. Lett. 96 (2006) (Art. No. 123901).
[38] A. Taflove, S.C. Hagness, Computational Electrodynamics: The Finite-Difference Time-Domain Method, Artech House, Norwood, 2005.